A Trajectory Controlled 48-to-24 V Resonant Switched Capacitor Converter with 98.7% Efficiency and Ultrafast Dynamic Response

Hélène T.W. Ma Yang
Edward S. Rogers Sr. Department of Electrical & Computer Engineering
University of Toronto
Toronto, Canada
helenetw.mayang@mail.utoronto.ca

Liang Wang
School of Information Science and Technology
ShanghaiTech University
Shanghai, China
wangliang1@shanghaitech.edu.cn

Haoyu Wang
School of Information Science and Technology
ShanghaiTech University
Shanghai, China
wanghy@shanghaitech.edu.cn

Wai Tung Ng
Edward S. Rogers Sr. Department of Electrical & Computer Engineering
University of Toronto
Toronto, Canada
ngwt@ece.utoronto.ca

2025 IEEE Applied Power Electronics Conference and Exposition (APEC) | 979-8-3315-1611-6/25/$31.00 ©2025 IEEE | DOI: 10.1109/APEC48143.2025.10977433

***Abstract*—Resonant converters have high power conversion efficiency and can achieve soft switching over a wide range of load conditions. However, during load transients, mismatches between the current provided by the resonant tank and the load current can cause abrupt voltage changes, affecting stability. Maintaining stable output voltage requires a large output capacitance, increasing cost and size. By controlling the trajectory of the resonant tank, rapid recovery after each load transient can be achieved. This work proposes a trajectory control method for a 48-to-24 V resonant switching capacitor converter to improve the transient response performance with a maximum load current of 20 A and output power of 480 W, a 90% reduction in output capacitance for the same output voltage ripple can be achieved with a peak efficiency of 98.7% and a very fast transient recovery of under 300 ns.**

Keywords—dynamic response, load transient, resonant series capacitor, trajectory control

I. Introduction

The Information Age is ushering in an unprecedented increase in data generation, processing, and storage requirements. This trend has been intensified by the recent rise of cloud computing, big data processing, and artificial intelligence (AI). The surge in data volume has placed immense pressure on data centers, which form the core of the digital infrastructure [1]. In 2022, data centers consumed no less than 500 TWh of energy globally. The International Energy Agency (IEA) conservatively projects that this consumption will increase to more than 800 TWh by 2026 [2]. With current power grids nearing their capacity limits, upgrading the existing infrastructure is a costly venture. Therefore, data centers must leverage technological advances to meet the growing demands for ever higher processing speeds while maintaining energy efficiency and reliability. Moreover, the conventional 12 V bus architecture in data centers is gradually being replaced by the 48 V bus architecture [3]. This upgrade is part of the shift to next-generation data centers. The 48 V architecture reduces losses but also introduces additional challenges, particularly for onboard power supplies (OPS).

Fixed-ratio buck converters are crucial in two-stage data center OPS. These power architectures feature a primary stage DC converter. This primary stage reduces the step-down requirement for secondary stage converters. The primary stage DC converter uses simple, efficient topologies with high efficiency, high power density, and simple control schemes [4]. Improving the transient response speed is crucial for improving the power density of the entire converter system. Faster response reduces the number of bus capacitors between the two stages, hence increasing the power density [5]. Common resonant converters in data center power supplies include LLC converters and resonant switching capacitor (RSC) converters. For isolated LLC converters, control methods have been proposed by Virginia Tech researchers in [6]-[9] to enhance its transient response. However, the transformer limits its efficiency. Non-isolated topologies such as the RSC converters are simpler and feature fewer components, allowing higher efficiency and power density. Optimized control can also enable zero current switching (ZCS) for soft switching. A single resonant unit in RSC converters achieves a 2:1 step-down ratio. Multiple units in series or switched tank converters can achieve higher ratios. However, additional components limit power density and efficiency. Optimized control for resonant RSC converters can modulate the output voltage and enhance performance [10], [11]. A few studies have addressed trajectory control for non-

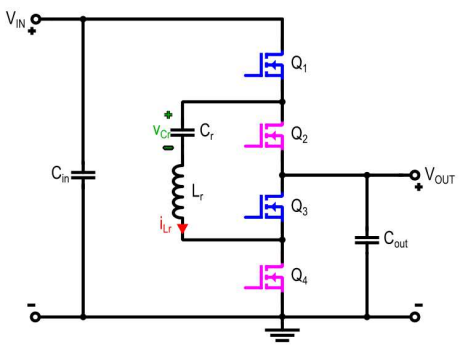

Fig. 1. The proposed resonant switched capacitor converter topology.

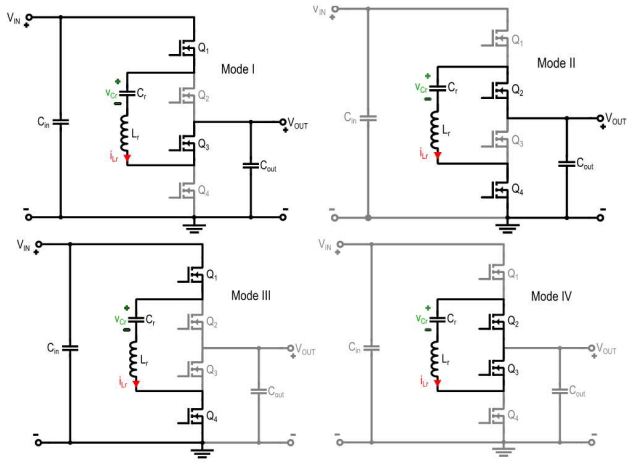

Fig. 2. Operation modes of the resonant switched capacitor converter.

isolated resonant RSC converters [12], [13]. Work by Sim *et al.* has reported V_{OUT} regulation using such control [14].

This paper proposes a trajectory control method for RSC converters to improve transient response performance. The organization is as follows: Section II introduces the circuit topology, describes the RSC converter's operation principles, and explains the trajectory control method. Section III presents the simulation results. Section IV provides the experimental results. Section V concludes the paper.

II. Circuit Topology, Operation Principles, and Trajectory Control

A. Circuit Topology

The topology of an RSC converter is shown in Fig. 1. It features four series-connected MOSFETs $Q_1 - Q_4$. A resonant tank is formed by the resonant capacitor C_r and resonant inductor L_r. The input and output capacitors C_{in} and C_{out} are sufficiently large such that the input and output voltages can be assumed to be constant during steady-state and transient operations.

B. Steady State Analysis

The RCS converter has two steady-state modes of operation, shown in Fig. 2. In Mode I, switches Q_1 and Q_3 conduct. The resonant tank is connected to the input power source and output load. The voltage across the resonant tank is $V_{IN} - V_{OUT}$. In Mode II, switches Q_2 and Q_4 conduct. The resonant tank is connected across output load. The voltage across the resonant tank is V_{OUT}. Fig. 3 shows the steady-state waveforms of the RCS converter. The duty cycle D for transistors $Q_1 - Q_4$ is 50%. The adjacent switches conduct in a complementary manner with a certain deadtime to prevent shoot through current.

The resonant tank, comprising of resonant capacitor C_r and resonant inductor L_r, has a resonant frequency f_r which can be expressed as:

$$f_r = \frac{1}{2\pi\sqrt{L_r \cdot C_r}}. \tag{1}$$

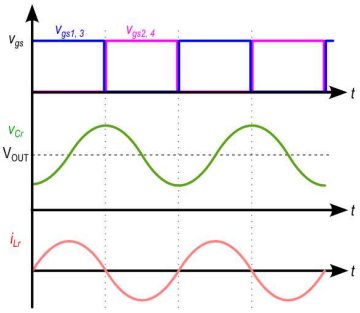

Fig. 3. Steady-state waveforms of the resonant switched capacitor converter.

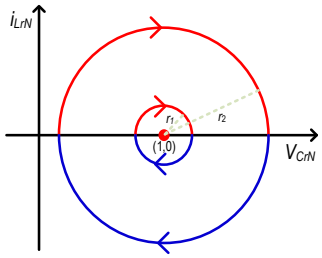

Fig. 4. Steady-state trajectory waveform of the resonant switched capacitor converter.

During mode transitions, the resonant inductor current $i_{Lr}(t)$ decreases to zero. This behavior achieves ZCS, reduces switching losses, and improves efficiency. The starting times of Mode I and II are defined as t_0 and t_1, respectively. The resonant inductor current $i_{Lr}(t)$ and capacitor voltage $v_{Cr}(t)$ over a full cycle can be expressed as:

$$i_{Lr}(t) = i_{Lr}(t_0)\cos[\omega(t-t_0)] - \frac{v_{Cr}(t_0) - V_{OUT}}{Z_0}\sin[\omega(t-t_0)], \tag{2}$$

$$v_{Cr}(t) = i_{Lr}(t_0)Z_0\sin[\omega(t-t_0)] + (v_{Cr}(t_0) - V_{OUT})\cos[\omega(t-t_0)] + V_{OUT}. \tag{3}$$

The state-plane analysis can be performed by normalizing the resonant inductor current and capacitor voltage. (2) and (3) are obtained after normalizing all voltages with respect to V_{OUT} and all currents with respect to V_{OUT}/Z_0. The normalized resonant trajectory is plotted in Fig. 4.

$$I_{LN} = I_{L0N}\cos\theta - (V_{C0N} - 1)\sin\theta, \tag{4}$$

$$V_{CN} = I_{L0N}\sin\theta + (V_{C0N} - 1)\cos\theta + 1. \tag{5}$$

$$I_{LN}{}^2 + (V_{CN} - 1)^2 = I_{L0N}{}^2 + (V_{C0N} - 1)^2 = (V_{C0N} - 1)^2. \tag{6}$$

In the normalized resonant trajectory plotted in Fig. 4, the horizontal axis represents the normalized capacitor voltage V_{CrN}. The vertical axis represents the normalized inductor current I_{LrN}. The trajectories are circles centered at $(1, 0)$. The radii are determined by different load conditions. The radius r of the circle can be expressed as:

$$r = 1 - V_{C0N} = \frac{Z_0\, I_{OUT}\, \pi}{2\, V_{OUT}}. \tag{7}$$

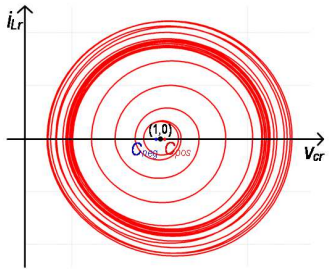

Fig. 5. Trajectory waveforms of the resonant switched capacitor converter with open-loop fixed-frequency control during load step-up.

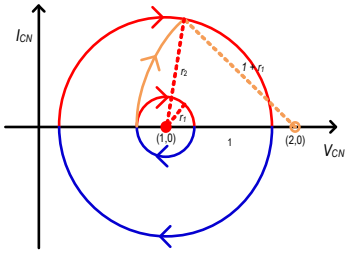

Fig. 6. Optimized trajectory waveform of the resonant switched capacitor converter during load step-up.

C. Transient State Analysis

During a load transient, the output voltage response is influenced by the converter's output impedance. Although the output voltage can eventually stabilize, a sudden load increase or decrease can cause mismatches between the inductor current and the load demand. This mismatch leads to temporary drops or overshoots in the output voltage. These output voltage changes affect stability and require additional output capacitors to maintain a steady voltage. However, adding capacitors increases cost and system size, which is undesirable for data center OPS.

The output voltage V_{OUT} deviates from the steady-state output voltage $V_{OUT,st}$ during load transients. The trajectory of the RSC converter during a load step-up transient is shown in Fig. 5. As the load current suddenly increases, V_{OUT} decreases. The trajectory on the positive half-cycle is thus $(V_{IN} - V_{OUT})/V_{OUT,st} > 1$, shifting to the right. Similarly, the trajectory on the negative half-cycle is $V_{OUT}/V_{OUT,st} < 1$, shifting to the left. In both cases, the radius will increase as per (7). After multiple cycles, the trajectory expands outward from smaller inner circles to larger outer circles. The resonant tank can balance the energy mismatch between the input and load demands. This mismatch leads to temporary ringing and overshoot at the output voltage. Therefore, traditional open-loop control with fixed frequency typically exhibits slow transient recovery and large voltage fluctuations during load changes.

To improve the transient performance of the RSC converter, a trajectory control scheme is proposed. During steady-state operation, an open-loop fixed-frequency control method is used to maintain the switching frequency to be the same as the resonant frequency. During transient operation, an optimized trajectory control method predicts the trajectory before and after the load variation. It adjusts the control signal immediately after switching and accurately generates the corresponding control signal. This allows the resonant tank state to follow the optimal trajectory in the shortest time possible. Doing so ensures fast switching between LO- and HI-load states, reduces the transient response time, minimizes output voltage ripple, and smooths the trajectory. Fig. 6 shows the optimized transient trajectory.

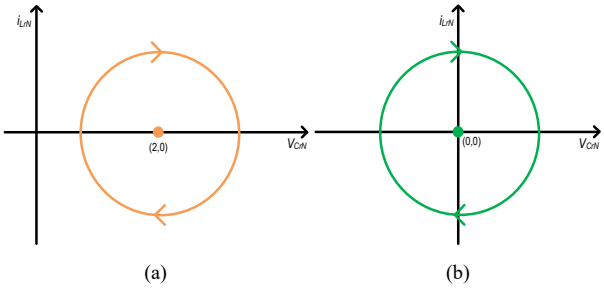

Fig. 7. Trajectory waveforms for (a) Mode III and (b) Mode IV.

To implement this trajectory control, Modes III and Mode IV are introduced, as shown in Fig. 7. In Mode III, switches Q_1 and Q_4 conduct. The resonant tank is connected to the input voltage. The resonant tank's voltage of $V_{IN} = 2\,V_{OUT}$ allows its energy to change rapidly. In Mode IV, switches Q_2 and Q_3 conduct. There is zero voltage across the resonant tank. The starting times of Mode III and IV are defined as t_0 and t_1, respectively. The resonant inductor current $i_{Lr}(t)$ and capacitor voltage $v_{Cr}(t)$ over a full cycle can be expressed as:

$$i_{Lr}(t) = i_{Lr}(t_0)\cos[\omega(t-t_0)] - \frac{V_{IN} - v_{Cr}(t_0)}{Z_0}\sin[\omega(t-t_0)]\,, \tag{7}$$

$$v_{Cr}(t) = i_{Lr}(t_0)\,Z_0\sin[\omega(t-t_0)] + (v_{Cr}(t_0) - V_{IN})\cos[\omega(t-t_0)] + V_{IN}\,. \tag{8}$$

Normalizing all voltages with respect to V_{OUT} and all currents with respect to V_{OUT}/Z_0, (7) and (8) can be rewritten and combined in (9). The trajectory with its center at $(2,0)$ is plotted in Fig. 7 (a). Equation (10) shows the trajectory radius.

$$I_{LN}{}^2 + (V_{CN} - 2)^2 = I_{L0N}{}^2 + (V_{C0N} - 2)^2. \tag{9}$$

$$r = \sqrt{I_{L0N}{}^2 + (V_{C0N} - 2)^2}\,. \tag{10}$$

Similarly for Mode IV, the resonant inductor current $i_{Lr}(t)$ and capacitor voltage $v_{Cr}(t)$ over a full cycle and the trajectory radius can be expressed as (11)-(13). Fig. 7 (b) shows the Mode IV's trajectory.

$$i_{Lr}(t) = i_{Lr}(t_0)\cos[\omega(t-t_0)] - \frac{v_{Cr}(t_0)}{Z_0}\sin[\omega(t-t_0)]\,, \tag{11}$$

$$v_{Cr}(t) = i_{Lr}(t_0)\,Z_0\sin[\omega(t-t_0)] + v_{Cr}(t_0)\cos[\omega(t-t_0)]\,. \tag{12}$$

$$I_{LN}{}^2 + V_{CN}{}^2 = I_{L0N}{}^2 + V_{C0N}{}^2. \tag{13}$$

$$r = \sqrt{I_{L0N}{}^2 + V_{C0N}{}^2}\,. \tag{14}$$

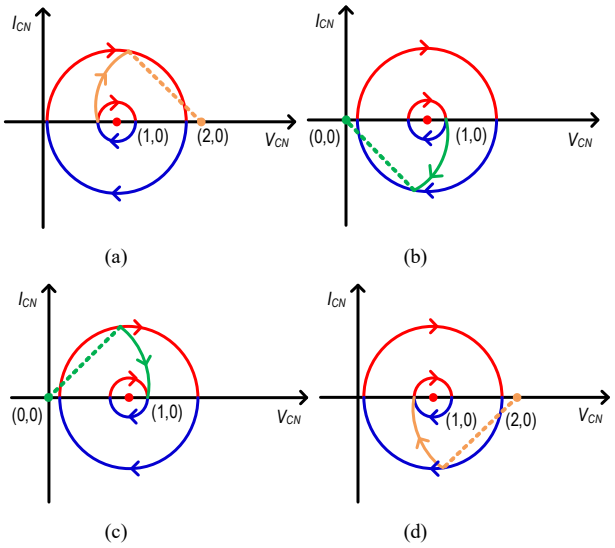

Fig. 8. Proposed transient trajectory methods for (a) positive half-cycle load step-up, (b) negative half-cycle load step-up, (c) positive half-cycle load step-down, and (d) negative half-cycle load step-down.

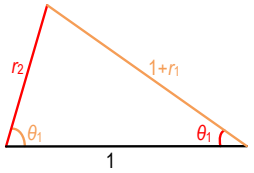

Fig. 9. Geometric relations for the transient trajector control strategy

D. Trajectory Control

Fig. 9 illustrates the proposed trajectory control principle. The control strategy can be divided into four cases depending on the load variation and the switching within the positive or negative half-cycle.

a) *Load step-up during positive half-cycle:* When the inductor current reaches zero, the RSC converter switches from Mode II to Mode III. The resonant tank energy increases rapidly until it matches the required energy. Then, the trajectory returns to the steady-state trajectory Mode I and switches between Modes I and II.

b) *Load step-up during negative half-cycle:* When the inductor current reaches zero, the RSC converter switches from Mode I to Mode IV. The trajectory continues in Mode IV until it reaches the steady-state trajectory Mode II and switches between Modes I and II.

c) *Load step-down during positive half-cycle:* After some time in Mode I, the system transitions to Mode IV. The resonant tank trajectory then follows Mode IV until it aligns with the steady-state trajectory of Mode II. When the inductor current reaches zero, the trajectory returns to Mode II and completes the transient response.

d) *Load step-down during negative half-cycle:* After some time in Mode II, the system transitions to Mode III. The resonant tank trajectory then follows Mode III until it aligns with the steady-state trajectory of Mode I. When the inductor current reaches zero, the trajectory returns to Mode I and completes the transient response.

Precise timing during transient switching is crucial to trajectory control, as shown in Fig. 8. Accurately calculating the durations of different modes during the transient process is critical for achieving rapid trajectory transitions. Taking the load step-up scenario as an example, Modes III and I's duration must be calculated accurately. By analyzing the geometrical relationships in Fig. 8, the geometric relationships of Fig. 9 can be obtained. r_1 and r_2 represent the radii of the trajectories in the steady-state Modes II and I, respectively. I_{OUT1} represents the load current during LO-load. I_{OUT2} represents the load current during HI-load. Note that LO- and HI-loads refer to the relative load currents before and after the change.

$$r_1 = \frac{Z_0 I_{OUT1} \pi}{2\, V_{OUT}}, \qquad r_2 = \frac{Z_0 I_{OUT2} \pi}{2\, V_{OUT}} \tag{15}$$

The triangle's sides are $(1 + r_1)$, r_2, and 1. Using the cosine rule, the angles θ_1 and θ_2 can be derived with θ_1 corresponding to the duration of the transition mode.

$$\theta_1 = arccos \frac{1 + (1 + r_1)^2 - r_2^2}{2\,(1 + r_1)}, \qquad \theta_2 = arccos \frac{1 + r_2^2 - (1 + r_2)^2}{2\, r_2} \tag{16}$$

The time corresponding to Mode III (t_1) and to Mode I (t_2) during the load step-up transient process can be derived as:

$$t_1 = \frac{\theta_1}{2\pi} T_s, \qquad t_2 = \frac{\theta_2}{2\pi} T_s \tag{17}$$

Therefore, with knowledge of the load current before and after transient switching, the control duration of each mode can be determined. This allows for rapid transient response and helps reduce the output capacitor size. Fig. 10 shows the control strategy. Fig. 11 depicts the trajectory control flowchart. When the output voltage is stable and the load current ripple is not severe, steady-state control is used. This maintains the converter's operation at steady-state, ensuring stability at the output voltage without being affected by load variations.

When significant load current changes are detected, transient trajectory control is activated. First, the load current is sampled to obtain the values for I_{OUT1} and I_{OUT2}. Based on the corresponding equations, the duration of each transient mode at both ends of the process is calculated. The system determines whether the converter is undergoing a load step-up or step-down process by comparing $I_{OUT1}$and I_{OUT2}. Next, the system checks whether it is in a positive half-cycle or a negative half-cycle based on the current operating state. These actions require real-time current monitoring. After completing transient trajectory control, the system exits transient mode and returns to steady-state fixed-frequency operation until the next transient load disturbance is detected.

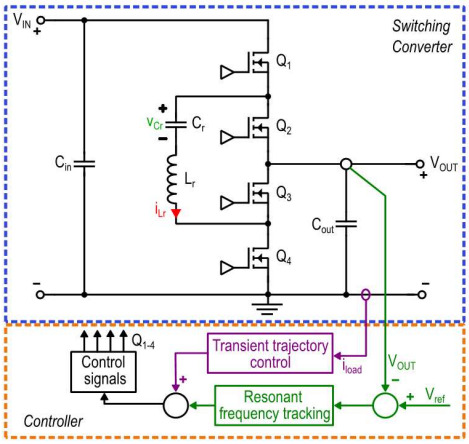

Fig. 10. Control strategy of the resonant switched capacitor converter.

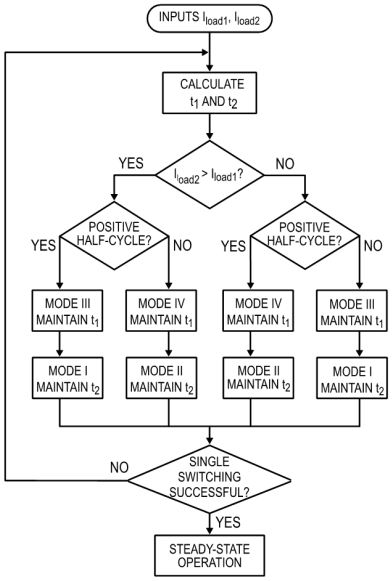

Fig. 11. Flowchart of the transient trajectory control.

III. Simulation Results

The proposed transient trajectory control is verified through PSIM simulations. The verification uses the example of load step-up from 6 A to 24 A during the positive half cycle. Fig. 12 shows the simulated waveforms using the traditional fixed-frequency control method. The simulation results show that when the load changes significantly under open-loop fixed-frequency control, the output voltage fluctuates considerably. The peak-to-peak amplitude is about 0.5 V. It takes about 700 µs for the voltage to return to steady state. The inductor current and capacitor voltage exhibit large oscillations. These oscillations could affect system lifespan and stability.

Fig. 13 shows the transient switching control signals. The resulting circuit waveforms are illustrated in Fig. 14. Using trajectory control, the inductor current quickly charges and transitions from LO- to HI-load in under 300 ns. There is little fluctuation in the voltage across the output capacitor. The

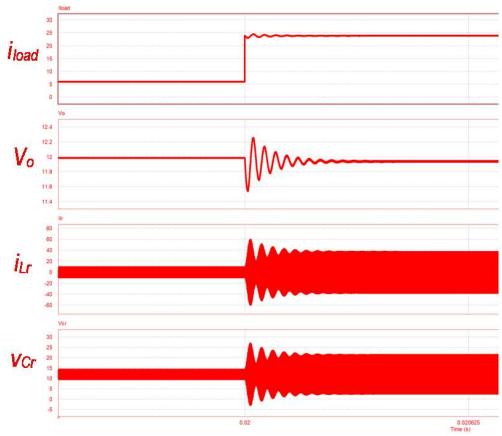

Fig. 12. Transient time-domain waveforms with conventional fixed-frequency during load step-up.

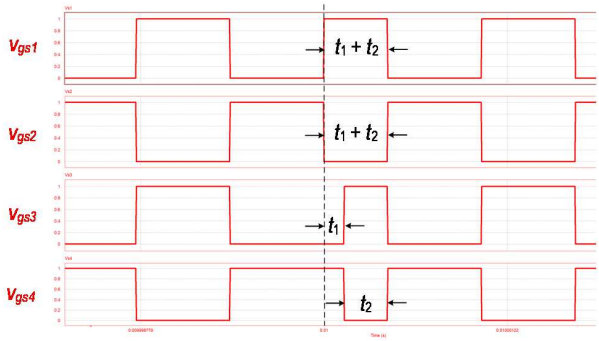

Fig. 13. Control signals during transient for trajectory control.

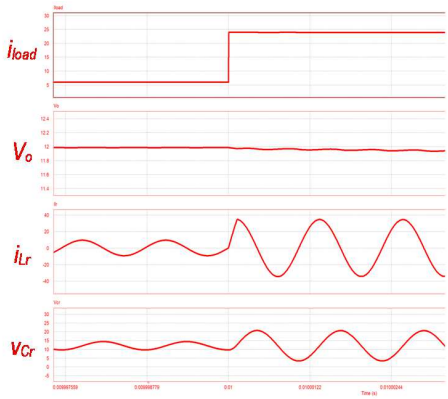

Fig. 14. Simulated time-domain transient waveforms with trajectory control.

proposed trajectory control method greatly reduces the output voltage fluctuation amplitude during sudden load changes.

Comparing the proposed trajectory control with traditional fixed-frequency open-loop control through simulation, the proposed method significantly reduces the voltage ripple during load step changes. It allows a 90% reduction in the output capacitance compared to the conventional control method. These reductions further lower the costs and the converter sizes.

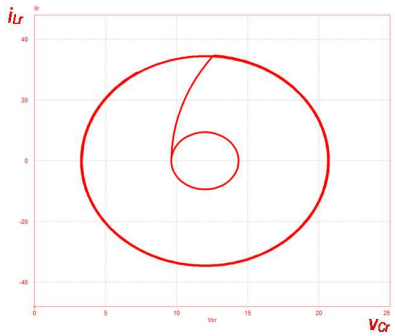

Fig. 15. Simulated transient trajectory waveform during load step-up.

Using time-domain waveforms, the trajectory waveform is shown in Fig. 15. Trajectory control rapidly transitions the resonant tank from the inner LO-load circle to the outer HI-load circle in a single-step operation. With precise control and matching, there is ideally no overshoot nor oscillation. This improves component stability.

IV. Experimental Results

To verify the effectiveness of the proposed control scheme, an RSC converter with a rated input of 48 V and a rated output of 24 V was designed. The circuit parameters are shown in Table I. The prototype converter is shown in Fig. 16. Two half-bridge drivers are used. Bootstrapping supplies the gate drive circuits for the switching devices.

Fig. 17 shows the steady-state experimental waveforms of the resonant capacitor voltage and resonant inductor current. Since the resonant frequency matches the switching frequency, the resonant inductor current and resonant capacitor voltage exhibit ideal sinusoidal waveforms. This ensures zero current during switching transitions, achieving ZCS soft-switching. In low-voltage and high-current applications, ZCS soft-switching helps to reduce switching losses and improve efficiency.

The RSC converter's steady-state efficiency achieves a peak efficiency of 98.7%, shown in Fig. 18. Under full load conditions, the converter reaches an efficiency of 97.5%, despite increased conduction losses. This is due to its simple topology, non-isolated structure, and soft switching characteristics.

TABLE I. RSC Converter Parameters

Components	Values
Input voltage V_{IN}	48 V
Output voltage V_{OUT}	24 V
Resonant capacitor C_r	5.2 µF
Resonant inductor L_r	100 nH
Switching frequency f_s	220 kHz
Output capacitance C_{OUT}	100 µF
Load current I_{OUT}	0-20 A

The output voltage waveform during transient load changes with trajectory control was verified experimentally. Fig. 19 shows the transient time-domain waveforms and trajectory for a load step-up from 5 A to 15 A during the positive half-cycle. The settling time after load transient is 260 ns. The experimental results show that the resonant inductor current rapidly charges

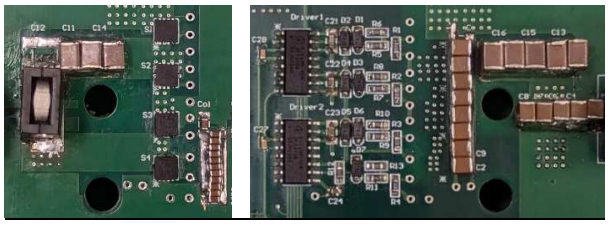

Fig. 16. The proposed resonant switched capacitor converter.

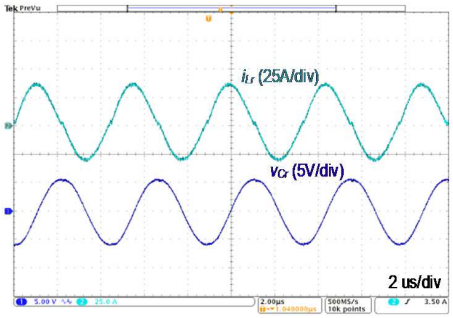

Fig. 17. Experimental steady-state waveforms.

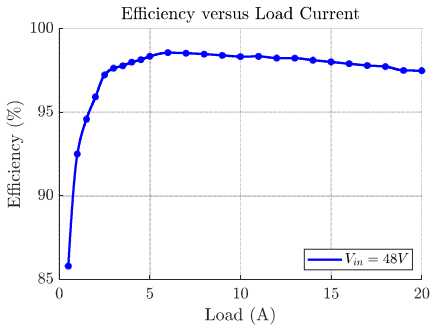

Fig. 18. A plot of the power conversion efficiency versus load current.

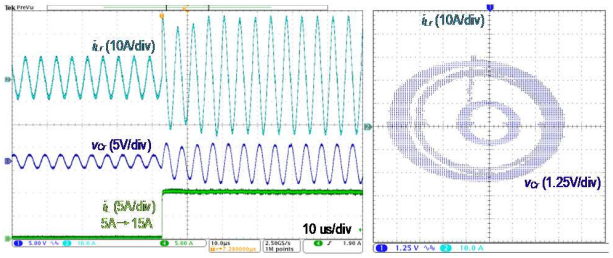

Fig. 19. Experimental waveforms of the trajectory control during negative half-cycle at load step-up.

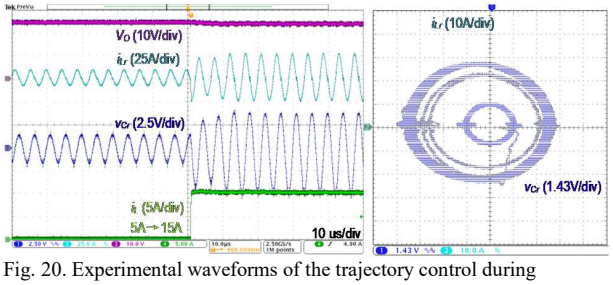

Fig. 20. Experimental waveforms of the trajectory control during negative half-cycle at load step-up.

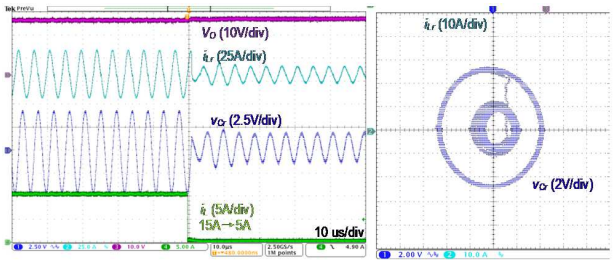

Fig. 21. Experimental waveforms of the trajectory control during positive half-cycle at load step-down.

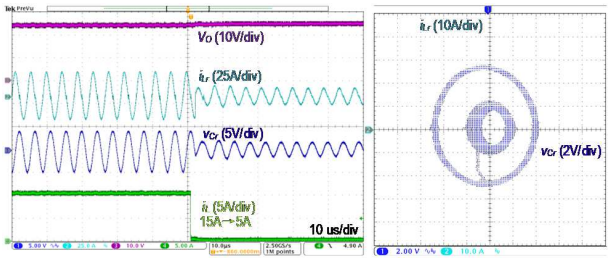

Fig. 22. Experimental waveforms of the trajectory control during negative half-cycle at load step-down.

during the transient mode to match the load current. The trajectory diagram shows a rapid trajectory transition during the LO-load to HI-load jump. Minor oscillations were observed during the experiment, but the output voltage returned to the set value after a short period.

Similarly, Fig. 20 shows the transient time-domain waveforms and trajectory for a load step-up from 5 A to 15 A during the negative half-cycle. Fig. 21 illustrates the transient time-domain waveforms and trajectory for a load step-down from 15 A to 5 A during the positive half-cycle. Finally, Fig. 22 presents the transient time-domain waveforms and trajectory for a load step-down from 15 A to 5 A during the negative half-cycle. All four experiments demonstrate excellent transient response performance. The trajectory control maintains a stable output voltage with no significant fluctuations during large load transients.

V. Conclusions

A trajectory control strategy for the primary-stage RSC converter is proposed to improve transient response performance in data center applications. Two transitional modes are introduced to improve transient response speed. Control strategies are proposed for the four scenarios of transitions between positive and negative half-cycles and LO- and HI-load conditions. The mathematical principles underlying trajectory control provide a theoretical foundation for precise control. Experimental results verified the feasibility of the proposed control concept and compared it with the traditional open-loop fixed-frequency control strategy. Under transient load conditions, the proposed control method demonstrated a 90% reduction in output capacitance for the same output voltage ripple, highlighting the validity of the proposed control strategy.

Acknowledgment

This project was made possible by financial support from the Natural Sciences and Engineering Research Council of Canada.

References

[1] A. Shehabi, S. J. Smith, E. Masanet, and J. Koomey, 'Data center growth in the United States: decoupling the demand for services from electricity use', *Environ. Res. Lett.*, vol. 13, no. 12, p. 124030, Dec. 2018, doi: 10.1088/1748-9326/aaec9c.

[2] 'Electricity 2024 – Analysis and forecast to 2026', IEA. Accessed: Sep. 09, 2024. [Online]. Available: https://www.iea.org/reports/electricity-2024

[3] P. Sandri, 'Increasing Hyperscale Data Center Efficiency: A Better Way to Manage 54-V\48-V-to-Point-of-Load Direct Conversion', *IEEE Power Electron. Mag.*, vol. 4, no. 4, pp. 58–64, Dec. 2017, doi: 10.1109/MPEL.2017.2760113.

[4] K. Kesarwani and J. T. Stauth, 'The direct-conversion resonant switched capacitor architecture with merged multiphase interleaving: Cost and performance comparison', in *2015 IEEE Applied Power Electronics Conference and Exposition (APEC)*, Mar. 2015, pp. 952–959. doi: 10.1109/APEC.2015.7104464.

[5] A. Borzooy, S. A. Khajehoddin, M. Karimi-Ghartemani, and M. Ebrahimi, 'Alternative Control Approach to Achieve Fast Load-Transient Responses in DC–DC Converters', *IEEE Trans. Ind. Electron.*, vol. 68, no. 12, pp. 12668–12678, Dec. 2021, doi: 10.1109/TIE.2020.3040675.

[6] R. Oruganti, J. J. Yang, and F. C. Lee, 'Implementation of optimal trajectory control of series resonant converter', in *1987 IEEE Power Electronics Specialists Conference*, Jun. 1987, pp. 451–459. doi: 10.1109/PESC.1987.7077214.

[7] W. Feng, F. C. Lee, and P. Mattavelli, 'Optimal Trajectory Control of Burst Mode for LLC Resonant Converter', *IEEE Trans. Power Electron.*, vol. 28, no. 1, pp. 457–466, Jan. 2013, doi: 10.1109/TPEL.2012.2200110.

[8] C. Fei, Q. Li, and F. C. Lee, 'Digital Implementation of Light-Load Efficiency Improvement for High-Frequency LLC Converters With Simplified Optimal Trajectory Control', *IEEE J. Emerg. Sel. Top. Power Electron.*, vol. 6, no. 4, pp. 1850–1859, Dec. 2018, doi: 10.1109/JESTPE.2018.2832135.

[9] A. Nabih, M. H. Ahmed, Q. Li, and F. C. Lee, 'Transient Control and Soft Start-Up for 1-MHz LLC Converter With Wide Input Voltage Range Using Simplified Optimal Trajectory Control', *IEEE J. Emerg. Sel. Top. Power Electron.*, vol. 9, no. 1, pp. 24–37, Feb. 2021, doi: 10.1109/JESTPE.2020.2973660.

[10] Y. P. B. Yeung, K. W. E. Cheng, S. L. Ho, K. K. Law, and D. Sutanto, 'Unified analysis of switched-capacitor resonant converters', *IEEE Trans. Ind. Electron.*, vol. 51, no. 4, pp. 864–873, Aug. 2004, doi: 10.1109/TIE.2004.831743.

[11] K. K. Law, K. W. E. Cheng, and Y. P. B. Yeung, 'Design and analysis of switched-capacitor-based step-up resonant converters', *IEEE Trans. Circuits Syst. Regul. Pap.*, vol. 52, no. 5, pp. 943–948, May 2005, doi: 10.1109/TCSI.2004.840482.

[12] J. Caro, J. Mayo-Maldonado, J. Valdez-Resendiz, A. Alejo-Reyes, F. Beltran-Carbajal, and O. Lopez-Santos, 'An Overview of Non-Isolated Hybrid Switched-Capacitor Step-Up DC–DC Converters', *Appl. Sci.*, vol. 12, p. 8554, Aug. 2022, doi: 10.3390/app12178554.

[13] Y. Dong-Ying, K. Shih-Hao, S. Yong-Long, C. Huang-Jen, L. Kuo-Chi, and Y. Ta-Yung, 'An Improved 48-to-12V Series-Parallel Resonant Switched-Capacitor Converter for Data Center Applications', in *2021 IEEE International Future Energy Electronics Conference (IFEEC)*, Nov. 2021, pp. 1–6. doi: 10.1109/IFEEC53238.2021.9661888.

[14] S. Y. Sim, X. Zhang, J. Jiang, K. Wei, and C. Huang, 'A 94.7% Efficiency Direct-Step-Down Switched-Tank-Based 48V to 1V-3.3V Hybrid Converter with Constant-Resonant-Time Closed-Loop Control', in *2024 IEEE Applied Power Electronics Conference and Exposition (APEC)*, Feb. 2024, pp. 1344–1350. doi: 10.1109/APEC48139.2024.10509251.